Received: 29 November 2018 | Revised: 29 March 2019 | Accepted: 20 May 2019

DOI: 10.1002/jbm.a.36727

ORIGINAL ARTICLE

Regional gene therapy with 3D printed scaffolds to heal critical sized bone defects in a rat model

Ram Alluri[1] | Xuan Song[2] | Sofia Bougioukli[1] | William Pannell[1] | Venus Vakhshori[1] | Osamu Sugiyama[1] | Amy Tang[1] | Sang-Hyun Park[3] | Yong Chen[4] | Jay R. Lieberman[1]

[1]Department of Orthopaedic Surgery, Keck School of Medicine of the University of Southern California, Los Angeles, California

[2]Department of Industrial and Systems Engineering, The University of Iowa, Iowa City, Iowa

[3]Orthopaedic Institute for Children, J. Vernon Luck. Sr. Orthopaedic Research Center, Los Angeles, California

[4]Viterbi School of Engineering, University of Southern California, Los Angeles, California

Correspondence
Jay R. Lieberman, Department of Orthopaedic Surgery, Keck School of Medicine at USC, 1520 San Pablo Street, Suite 2000, Los Angeles, CA 90033.
Email: jay.lieberman@med.usc.edu

Funding information
Broad Stem Cell Foundation; Foundation for the National Institutes of Health, Grant/Award Number: R01AR057076

Abstract

The objective of the present study was to assess the ability of transduced rat bone marrow cells (RBMCs) that overexpress BMP-2 loaded on a three-dimensionally (3D) printed scaffold to heal a critical sized rat femoral defect. Tricalcium phosphate (TCP) scaffolds were 3D printed to fit a critical sized rat femoral defect. The RBMCs were transduced with a lentiviral (LV) vector expressing BMP-2 or GFP. The rats were randomized into the following treatment groups: (1) RBMC/LV-BMP-2 + TCP, (2) RBMC/LV-GFP + TCP, (3) nontransduced RBMCs + TCP, (4) TCP scaffold alone. The animals were euthanized at 12 weeks and evaluated with plain radiographs, micro-computed tomography (micro-CT), histology, histomorphometry, and biomechanically. Each LV-BMP-2 + TCP treated specimen demonstrated complete healing of the femoral defect on plain radiographs and micro-CT. No femurs healed in the control groups. Micro-CT demonstrated that LV-BMP-2 + TCP treated femoral defects formed 197% more bone volume compared to control groups ($p < 0.05$). Histologic analysis demonstrated bone formation across the TCP scaffold, uniting the femoral defect on both ends in the LV-BMP-2 + TCP treated specimens. Biomechanical assessment demonstrated similar stiffness ($p = 0.863$), but lower total energy to failure, peak torque, and peak displacement ($p < 0.001$) of the femurs treated with LV-BMP-2 + TCP when compared to the contralateral control femur. Regional gene therapy induced overexpression of BMP-2 via transduced RBMCs combined with an osteoconductive 3D printed TCP scaffold can heal a critically sized femoral defect in an animal model. The combination of regional gene therapy and 3D printed osteoconductive scaffolds has significant clinical potential to enhance bone regeneration.

KEYWORDS
3D printing, bone, regional gene therapy, scaffold, tissue engineering

1 | INTRODUCTION

The reconstruction of significant bone loss after trauma, revision joint arthroplasty, or failed spinal fusion are challenging problems in orthopedic surgery and can result in significant morbidity, healthcare resource utilization, and socioeconomic cost (Verettas, Galanis, Kazakos, Hatziyiannakis, & Kotsios, 2002). Successful reconstruction of large structural bone defects requires osteogenic cells, osteoinductive stimulus, and an osteoconductive scaffold over which new bone can be formed. Autologous bone grafting continues to remain

the gold standard as it provides all three requisites for bone regeneration; however, it is limited in availability and can result in harvest site complications such as long-lasting pain, infection, and nerve damage (Ahlmann, Patzakis, Roidis, Shepherd, & Holtom, 2002; Mastrogiacomo et al., 2005; Younger & Chapman, 1989). The use of bone allograft avoids donor site complications but allografts are limited in size, osteogenic potential, and carry a potential risk for disease transmission. Bone transport techniques allows for the reconstruction of diaphyseal bone defects but requires multiple surgeries, patient inconvenience related to external fixation, and has a high complication rate (Demiralp, Ege, Kose, Yurttas, & Basbozkurt, 2014). Recombinant bone morphogenetic protein-2 (rhBMP-2) is a potent osteoinductive growth factor and was initially thought to be an optimal bone graft substitute; however, it has largely failed to fulfill its clinical promise (Carragee, Hurwitz, & Weiner, 2011; Garrison et al., 2007). The efficacy of rhBMP-2 may be limited by its rapid release from the collagen sponge carrier and therefore large amounts of rhBMP-2 are required clinically to induce sufficient bone formation, which has been associated with complications such as ectopic bone formation and soft tissue swelling (Chan, Garland, Infante, Sanders, & Sagi, 2014; Jeon, Song, Kang, Putnam, & Kim, 2007; Lieberman, Daluiski, & Einhorn, 2002; Seeherman, Li, Bouxsein, & Wozney, 2010). The limitations of current treatment options have generated marked interest in developing translational bone regeneration strategies to safely and effectively heal large bone defects.

Ex vivo regional gene therapy is potentially a viable alternative as it allows the investigator to transduce a given stem cell type with a vector containing the cDNA for bone morphogenetic protein-2 (BMP-2) and transduced cells then overexpress BMP-2 and induce bone formation (Hsu et al., 2007; Ishihara, Zekas, Litsky, Weisbrode, & Bertone, 2010; Lieberman, Daluiski, Stevenson, et al., 1999; Peterson et al., 2005; Prockop, 1997; Shen et al., 2004). Several prior studies have investigated how to best optimize this process through variations in cell type, vector modification, and transduction methodology (Bougioukli, Evans, Alluri, Ghivizzani, & Lieberman, 2018; Virk et al., 2011). However, the cell carrier, or scaffold, used to deliver the transduced cells has received limited attention. Prior studies have utilized demineralized bone matrix (DBM), collagen sponges, and ceramic composites as scaffolds to deliver transduced cells after ex vivo gene therapy (Lieberman et al., 1999; Virk et al., 2011; Wang & Kanim, 2003). However, these scaffolds have been fabricated by traditional methods and therefore their properties such as pore size and three-dimensional (3D) microstructure were not necessarily optimized for cell communication, vascular ingrowth, and bone formation (Sanz-Herrera, Doblaré, & Garcia-Aznar, 2010; Warnke, Seitz, Warnke, et al., 2010; Woodfield et al., 2004). In addition, these materials may be cumbersome to use when treating large bone defects.

With the advent of 3D printing, increased attention has been focused on the design of osteoconductive scaffolds as 3D printing allows for the precise control of the scaffold via specific layer-by-layer material deposition allowing for customization of biomechanical properties such as elasticity and porosity, adhesive properties for cell-based strategies, and for the potential incorporation of growth factors to provide bioactivity (Lee et al., 2011). In addition, 3D printing allows for the customization of scaffolds to fit complex skeletal defects, which has substantial clinical applicability. The ideal scaffold for bone repair applications should be biocompatible with the transduced cells thereby allowing for cell adhesion and expansion, osteoconductive, and biodegradable (Castilho et al., 2014). Prior studies have evaluated the efficacy of bone formation when combining 3D printed scaffolds with growth factors such as rhBMP-2 (Lee, Deconde, Lee, et al., 2015; Shim et al., 2014; Temple et al., 2014; Wang et al., 2016). However, the clinical potential of this strategy may be limited as the osteoinductive signal generated by rhBMP-2 is likely not sustained over a sufficient period of time in vivo to induce healing of a large bone defect.

Combining ex vivo regional gene therapy with a 3D printed scaffold provides a sustained osteoinductive signal, through transduction of osteogenic cells, and a highly osteoconductive scaffold specifically designed to facilitate bone formation and transduced cell viability (Feeley et al., 2006). This multidisciplinary strategy is a potentially favorable approach to treat significant bone loss scenarios. The purpose of this study was to assess the capability of transduced rat bone marrow cells (RBMCs) producing BMP-2 loaded on a 3D printed osteoconductive scaffold to successfully repair a critically sized bone defect in a rat femur.

2 | MATERIALS AND METHODS

2.1 | 3D printed scaffold

Computed tomography (CT) scans of the intact femur of a 24-week-old male Lewis rat were taken as DICOM image files and converted into a 3D stereolithography (STL) file using commercial software (Mimics; Materialise NV, Leuven, Belgium) (Figure 1a). A 6 mm section of the mid diaphysis was taken from the model and multiple 700 μm holes were added to facilitate cellular communication and vascular ingrowth throughout the scaffold (Figure 1b) (Karageorgiou & Kaplan, 2005). The 700 μm pores were the only source of porosity in the scaffold.

A projection-based ceramic STL process was used to fabricate Tricalcium phosphate (TCP) scaffold structures to precisely fit a 6 mm rat femoral defect based on the DICOM image. This process creates a complex TCP structure via solidifying a viscous slurry-mixture of photocurable resin (Formlabs, Somerville, MA) and TCP powder (Ceramisys; Sintered beta-Tricalcium Phosphate, Sheffield, United Kingdom) with a customized ultraviolet (UV) light engine in a layer-by-layer fashion, followed by high-temperature post-processing for removing the resin and densifying the TCP particles (Song, Chen, Lee, Wu, & Cheng, 2015). More details about the process can be found in our previous work (Song et al., 2015).

2.2 | X-ray diffraction analysis

X-ray diffraction (XRD) (Ultima IV Diffractometer, Rigaku, Tokyo, Japan) analysis was performed to characterize the molecular compounds contained within the synthesized scaffold based on diffraction patterns. The 3D printed TCP scaffold was crushed into its powder

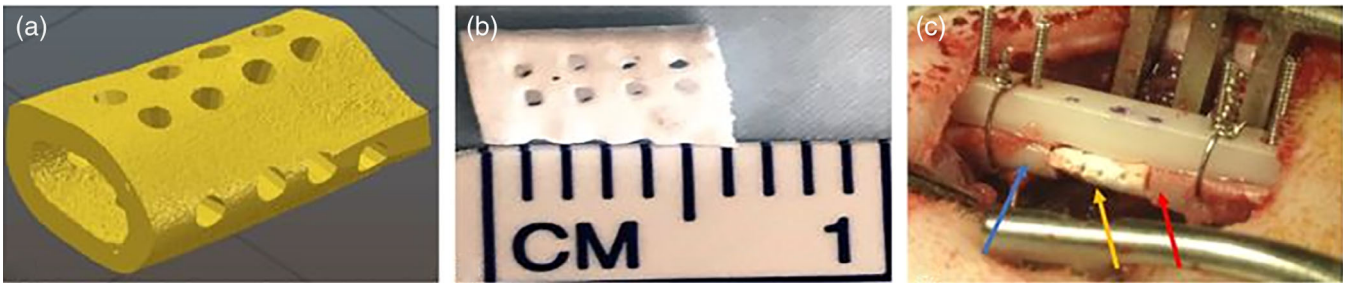

FIGURE 1 (a) Stereolithography (STL) file created from a computed tomography (CT) scan of a rodent femur. (b) Tricalcium phosphate (TCP) scaffold with 700 μm pores 3D printed to fit a critical sized rat femoral defect. (c) Intraoperative photograph demonstrating placement of the 3D printed TCP scaffold (yellow arrow) within the rat femoral defect (the blue arrow points to the distal femoral segment and the red arrow points to the proximal femoral segment)

form prior to XRD characterization. XRD was performed from 15° to 75° at a speed of 6° per minute (dpm). A zero diffraction slide was used to minimize background noise. Diffraction pattern analysis was completed using Jade 9 software (KS Analytical Systems, Aubrey, TX). A pure powder TCP sample from which the 3D printed TCP scaffold was synthesized served as a control. Figure of merit (FoM) was calculated for the crushed scaffold and the pure powder TCP sample to allow for comparisons of the composition.

2.3 | Rat bone marrow cell isolation and transduction

Rat bone marrow cells (RBMCs) were harvested from tibias and femurs of 8-week-old rats (Male Lewis Rats; Charles River Laboratories, Wilmington, MA) (Sugiyama et al., 2005). The resulting cell pellet was resuspended in Iscove's modified Dulbecco's media (IMDM) (ThermoFisher Scientific, Waltham, MA) and supplemented with 15% fetal bovine serum (FBS) (Omega Scientific, Tarzana, CA), streptomycin 100 μg/mL and penicillin 100 U/mL, and plated on a 100 mm dish for culture-expansion. When 90–100% confluent, adherent cells were trypsinized and passaged with plating 0.7 – 1 x 10 (Carragee et al., 2011) cells per dish. Passage 3 cells were transduced with a lentiviral vector carrying the cDNA for BMP-2 (LV-BMP-2) or green fluorescent protein (GFP) (LV-GFP) at a multiplicity of infection of 25 in the presence of 8 μg/mL polybrene (Sigma, St. Louis, MO).

2.4 | Study groups

There were four groups in the study, one experimental group (group 1) and three negative control groups (groups 2–4) (Table 1). Rats were randomly assigned to each group.

2.5 | Rat femoral defect model

The study was conducted in compliance with Institutional Animal Care and Use Committee (IACUC) regulations. A 23 mm × 4 mm × 4 mm polyethylene four-hole plate was secured to the left femur both proximally and distally with threaded wires and cerclage wires in a 12-week-old male Lewis rat. A standard 6 mm femoral defect was created with a high speed burr (Lieberman et al., 1999). This is a critical-sized defect and will not heal without a robust osteoinductive stimulus. The periosteum was removed and the intramedullary canals were flushed with normal saline solution to remove remaining osteoprogenitor cells from the defect site. The 3D printed TCP scaffold specifically designed to fit the femoral defect was injected with 5 million RBMCs diluted in phosphate-buffered saline (PBS) from groups 1–3 just before implantation or left empty for animals in group 4. The scaffold was then inserted into the bone defect (Figure 1c) and secured with two circumferential Vicryl sutures. Overlying muscle was closed with Vicryl suture further securing the scaffold in place. Animals were allowed to weight-bear immediately after surgery.

2.6 | Radiographic analysis

Plain radiographs of all operated femurs were taken at 4, 8, and 12 weeks after the surgical procedure using a Faxitron imaging system (Faxitron Bioptics, Tucson, AZ). The radiographs were assessed to determine whether the defect had healed. Three blinded observers graded healing of the defect from 0 to 5 where 0 represents no healing and 5 represents complete healing defined as bridging of both cortices (Lieberman et al., 1999). Radiographs taken at 8 and 12 weeks were graded.

2.7 | Microcomputed tomography

A microcomputed tomography (micro-CT) scan (μCT40, Scanco Medical, Bassersdorf, Switzerland) was performed on all of the operated femurs after euthanasia at 12 weeks to assess bone volume formed at the femoral defect (Virk et al., 2011). The amount of cortical bone and trabecular bone formed (bone volume) within the femoral defect region (tissue volume) was calculated after the TCP scaffold was digitally subtracted. The total volume of bone formation (bone volume fraction (BVF) = bone volume (BV)/tissue volume (TV)) was calculated and average BVF ratios were compared for each group.

2.8 | Histologic and histomorphometry

A total of 19 femurs were analyzed histologically (Table 1). Five-millimeter axial and transverse sections were cut, allowing for analysis

TABLE 1 Study groups and studies of the defects

Treatment group	# total defects	# that were studied radiographically	# that were studied with micro-CT	# that were studied histologically and histomorphometrically	# that were studied biomechanically
Group 1: LV-BMP2 + TCP scaffold	14	14	14	5	9
Group 2: LV-GFP + TCP scaffold	5	5	5	5	0
Group 3: Nontransduced RBMCs + TCP scaffold	5	5	4[a]	4[a]	0
Group 4: TCP scaffold without cells	5	5	5	5	0

[a]One rat (Rat 296) had failed fixation at the 8-week time point and was euthanized prior to the 12-week time point and therefore did not undergo micro-CT or histology staining.

TABLE 2 Radiographic outcomes

	4 weeks		8 weeks		12 weeks	
Treatment group	Score	# with complete healing	Score	# with complete healing	Score	# with complete healing
Group 1: LV-BMP2 + TCP scaffold	N/A	2 (14%)	4.78 ± 0.30	8 (57%)	4.93 ± 0.14	14 (100%)
Group 2: LV-GFP + TCP scaffold	N/A	0 (0%)	0.3 ± 0.32	0 (0%)	0.67 ± 0.71	0 (0%)
Group 3: Nontransduced RBMCs + TCP scaffold	N/A	0 (0%)	0.2 ± 0.32	0 (0%)	0.33 ± 0.19	0 (0%)
Group 4: TCP scaffold without cells	N/A	0 (0%)	0.9 ± 0.59	0 (0%)	1.07 ± 1.01	0 (0%)

in two planes with hematoxilin & eosin (H&E), Masson's trichrome, and tartrate-resistant acidic phosphatase (TRAP) staining. Each specimen was evaluated for the presence of cortical bridging across the femoral defect site, inflammation, and presence of osteoclasts.

Following staining, the axial images were analyzed with Bioquant analysis software (Bioquant Image Analysis, Nashville, TN) under 1× magnification. Bone area (BA) and tissue area (TA) were selected using the Bioquant software. The two axial histologic images were analyzed and the mean BA/TA ratio was averaged for each femur. Mean BA/TA ratios were calculated for each study group and compared.

2.9 | Biomechanical testing

The operative femur from nine specimens in the experimental group (group 1) underwent biomechanical testing. The contralateral, unoperated femur of each animal was also tested to serve as a control. The surrounding soft tissue, pins, wires, and plate were removed from each specimen prior to testing. Each specimen was frozen and then thawed right before testing. All testing was conducted on the same day to minimize variation due to temperature or biomechanical setup.

Each end of the specimen was potted in polymethylmethacrylate blocks and mounted on a torsional testing fixture such that the longitudinal bone axis was centered with the axis of torsion. The torsional testing fixture and specimen were attached to a universal testing machine (Minneapolis, MN). Using a rate of 15° per minute, the distal end of the specimen was internally rotated until bone failure. Torsional stiffness, maximum torque, peak displacement, and total energy for failure were calculated and the mean values for the operative and intact contralateral femurs were compared.

2.10 | Statistical analysis

Statistical analysis was performed using IBM SPSS Statistics 21. The results are given as mean and *SD*. The data were first checked for normality using Shapiro–Wilk test. One-way ANOVA and post-hoc analysis with Tukey's range test were done for comparisons in X-ray scores as well as BV and BVF between the different treatment groups. Biomechanical parameters between the operated and intact contralateral limbs were compared using Mann–Whitney *U* test.

3 | RESULTS

3.1 | Scaffold composition

The XRD pattern for the pure TCP powder was most similar to calcium phosphate with a FoM of 6.8 and 92% composition similarity. The XRD pattern for the 3D printed TCP scaffold was also most similar to calcium phosphate with a FoM of 7.5 and 92% composition similarity.

3.2 | Radiographic outcomes

All femurs (14 out of 14) in group 1 demonstrated complete healing of the bone defect at the 12-week time point with an average score of 4.93 ± 0.14 (Table 2 and Figure 2). Plain radiographs demonstrated robust bone formation around the 3D printed TCP scaffold and across the defect at 12 weeks. Prior to the 12 week time point, two femurs (14%) had healed at 4 weeks, and 8 femurs had healed at 8 weeks (57%). No femoral defects in groups 2–4 demonstrated evidence of complete radiographic healing at any time point. Healing grades of femurs in group 1 were significantly greater than those from groups

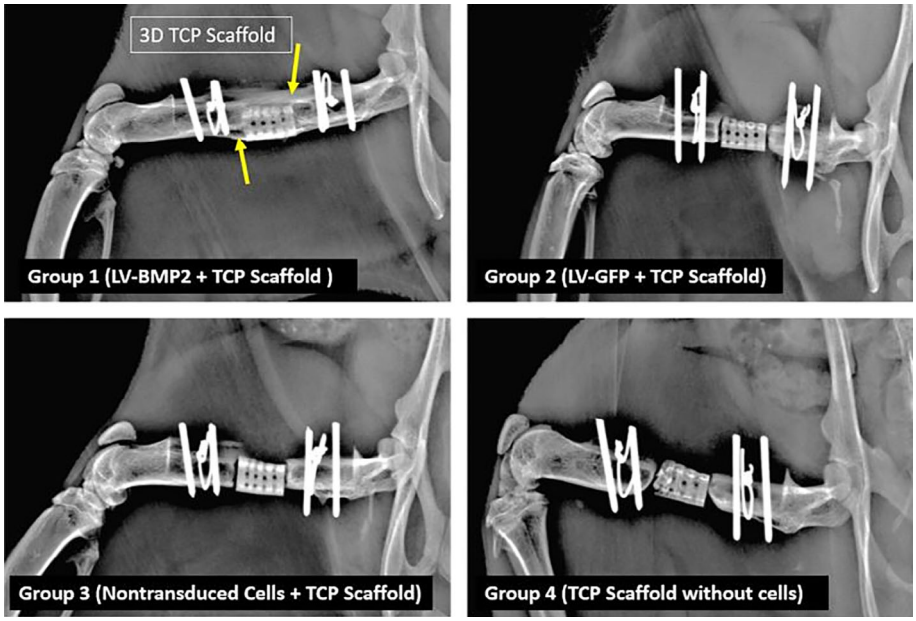

FIGURE 2 Representative plain radiographic images from groups 1–4 taken at 12 weeks after insertion of the 3D printed TCP scaffold. Only group 1 demonstrated complete healing of the defect. The yellow arrows illustrate bone surrounding the scaffold, bridging the defect proximally and distally

2–4 ($p < 0.001$) at the 8- and 12-week time points (Table 2). There was no significant difference in radiographic scores between groups 2–4 ($p > 0.05$) (Table 2). There was moderate interobserver agreement among the three reviewers who scored the radiographs (8-week kappa = 0.60, 12-week kappa = 0.61).

3.3 | Microcomputed tomography

At the 12-week time point, Micro-CT confirmed complete healing of all 14 femurs in group 1. No bone formation was noted within the defect in groups 2–4. Micro-CT demonstrated approximately fivefold greater BVF in group 1 compared to groups 2–4 ($p < 0.001$) (Figure 3). There was no significant difference in BVF between groups 2–4 ($p > 0.05$). The average BV/TV in group 1 was 25.33 ± 9.05%, 6.03 ± 3.34% in group 2, 4.10 ± 0.54% in group 3, and 6.20 ± 1.79% in group 4.

3.4 | Histology and histomorphometry

The femurs from group 1 demonstrated substantial trabecular bone formation across the scaffold–bone interface both proximally and distally (Figure 4). On cross-sectional samples, trabecular bone formed circumferentially around the entire 3D printed TCP scaffold in group 1. Groups 2–4 demonstrated minimal new bone formation at the scaffold-defect interface, and no bone formation surrounding the scaffold on cross-sectional imaging.

On H&E staining in one specimen from group 2 and a second from group 3, there was significant inflammatory cell infiltration and necrosis surrounding the pin sites. Both of these specimens had negative TRAP stains. TRAP staining around the proximal pin sites was positive in one specimen from group 2 and a second specimen from group 4; no significant inflammatory reaction in these two specimens was noted on H&E staining. No inflammatory reaction or TRAP positive specimens were noted in group 1.

Significant differences in bone formation between group 1 and groups 2–4 demonstrated on radiographs, micro-CT, and qualitative histology were confirmed with histomorphometric analysis. Total average bone volume induced by group 1 (BA/TA = 0.134 ± 0.056) was significantly greater than groups 2–4 ($p < 0.05$). Average BA/TA was 0.052 ± 0.022 in group 2, 0.056 ± 0.043 in group 3, and 0.035 ± 0.020 in group 4. There was no significant difference in BA/TA between groups 2–4 ($p > 0.05$).

3.5 | Biomechanics

The mean stiffness, total energy, peak torque, and peak displacement of the healed segmental defects from group 1 and the unoperated, contralateral femur are presented in Table 3. Stiffness between the healed defect and unoperated femur were similar ($p = 0.863$). Total energy to failure, peak torque, and peak displacement were significantly greater in the unoperated femur ($p < 0.001$). No defects in groups 2–4 demonstrated adequate bone formation and stability of the bone defect to undergo biomechanical testing.

3.6 | Complications

There were no complications in the LV-BMP2 + TCP scaffold group (group 1). One rat from group 3 died on postoperative day two likely secondary to complications from anesthesia; this rat was replaced. The proximal fixation in one rat in group 3 failed at 8 weeks and this rat was euthanized prior to the 12-week time point. In 3 rats (60%) in group 4, plain radiographs at 4, 8, and 12 weeks demonstrated migration of the TCP scaffold within the defect. This occurred because there was no bone healing in the defect. One rat from group 2 and one rat in group 4 were noted to have loose proximal pins at the time of limb harvest; these two rats had the positive TRAP staining on histology in the absence of significant inflammation, consistent with

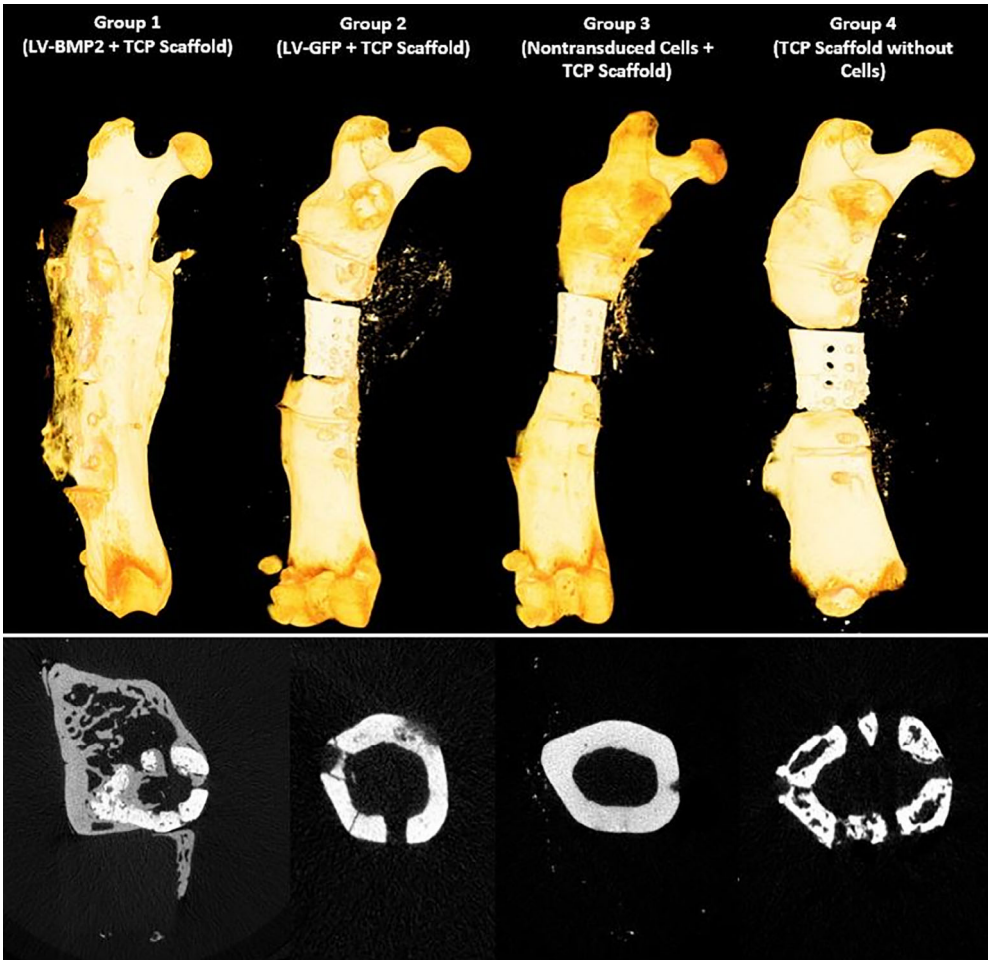

FIGURE 3 Representative micro-CT scans with three-dimensional reconstructions (top) and axial images (bottom) obtained from groups 1–4 after specimen harvest. Only group 1 demonstrated complete healing of the defect and on the axial image; circumferential bone can be seen surrounding the 3D printed TCP scaffold. No bone formed within the defect in groups 2–4

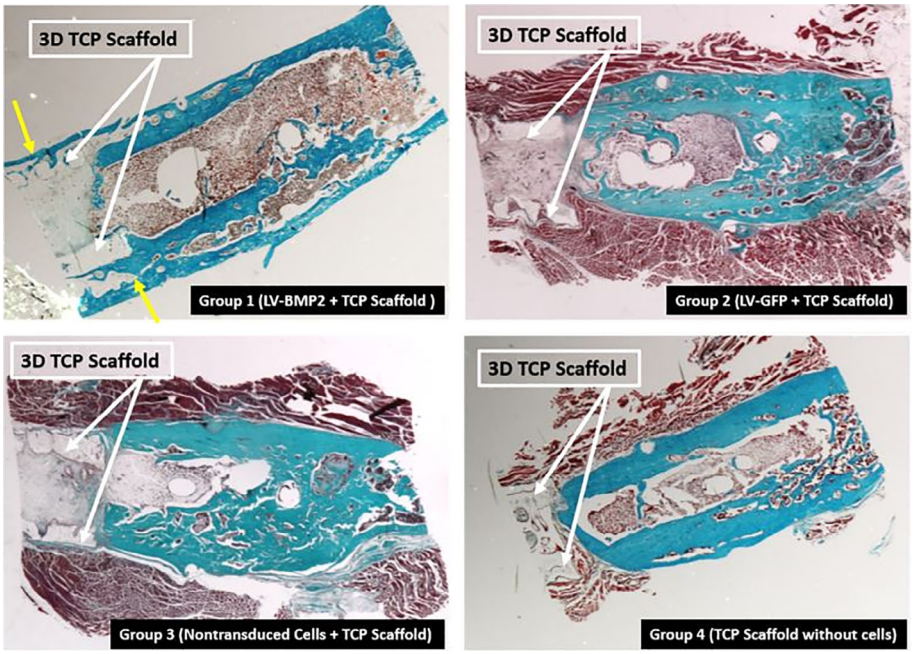

FIGURE 4 Select longitudinal histological cuts of the proximal scaffold-defect interface from groups 1–4. The samples are stained with Masson's trichrome stain. Only group 1 demonstrated trabecular bone formation (yellow arrows) within the 3D printed TCP scaffold (white arrows), uniting the scaffold to both ends of the defect. There is no notable trabecular bone in groups 2–4, and the TCP scaffold (white arrow) is mostly surrounded by muscle

aseptic osteolysis. Two additional rats, one from group 2 and one from group 3, were noted to have purulent material at the loose proximal pin sites at the time of limb harvest. During the course of the study, the pins became loose and the superficial tip of the pins migrated and violated the epidermal layer but this was not clearly evident during routine clinical inspection due to the rats' thick fur layer. The histologic sections of these two femurs revealed a significant inflammatory reaction but were TRAP negative.

TABLE 3 Biomechanics results of group 1 (LV-BMP2 + TCP scaffold)

Outcome	Experimental limb	Contralateral limb	*p*-value
Stiffness (nm/deg)	0.06 ± 0.02	0.06 ± 0.01	0.863
Total energy (nm·deg)	1.36 ± 0.68	3.66 ± 1.13	<0.001
Peak torque (nm)	0.36 ± 0.10	0.62 ± 0.11	<0.001
Peak displacement (deg)	8.36 ± 1.40	12.4 ± 2.42	<0.001

4 | DISCUSSION

There is an ongoing need for the development of tissue engineering strategies that allow for the reconstruction of significant bone loss after trauma, revision joint arthroplasty, or spinal pseudarthrosis. The majority of significant bone loss scenarios are treated with bone autograft or allograft. When large skeletal defects need to be reconstructed, bone autograft may be limited in supply, and bone allograft alone may not provide a sufficient osteogenic stimulus to produce adequate bone formation. Utilizing a multidisciplinary approach by combining ex vivo regional gene therapy and 3D printing represents a potentially favorable approach to treat significant bone loss scenarios as a continuous osteoinductive signal is provided by the transduced cells and the osteoconductive 3D printed scaffold serves as a carrier for localized delivery of the cells. The healing of these rat critical sized femoral defects demonstrates proof of concept that a tissue engineering strategy using regional gene therapy and 3D printing can induce robust osteogenesis.

The ideal combination of regional gene therapy and scaffold fabrication for bone regeneration remains unclear. The scaffold should serve several purposes including delivery of the transduced cells, ability to fit complex 3D skeletal defects, biocompatibility, controlled biodegradability, and high osteoconductivity. Previous regional gene therapy strategies for bone repair have used DBM, hydroxyapatite-TCP, and type I collagen sponge (Lieberman et al., 1999; Virk et al., 2011; Wang & Kanim, 2003). However, these studies all used traditionally fabricated scaffolds that cannot be easily adapted to fit the exact shape and size of large osseous defects. Prior studies have evaluated 3D printed scaffolds loaded with osteoinductive stimulants such as nontransduced stem cells or rhBMP-2 (Roskies et al., 2016; Temple et al., 2014). Only one study has evaluated the combination of regional gene therapy and a 3D printed scaffold; it demonstrated proof of concept that ectopic bone could be formed in a mouse muscle pouch; however, this study did not investigate the ability of the tissue engineering strategy to heal a stringent bone defect model (Alluri et al., 2018).

Prior studies from our lab have demonstrated the ability of regional gene therapy to heal critical sized bone defects (Lieberman et al., 1999; Peterson et al., 2005; Virk et al., 2011). In this study, we chose to use 3D printed scaffolds from TCP as it is structurally similar to cancellous bone, highly osteoconductive, and has been used in animal and clinical studies for bone repair/regeneration (Carrodeguas & De Aza, 2011; Dorozhkin, 2012; Esposito, Grusovin, Kwan, Worthington, & Coulthard, 2008; Wagoner Johnson & Herschler, 2011). In the current study, our slurry-based STL 3D-printing process was able to 3D print scaffolds that precisely fit the rat femoral defect while preserving the mineral properties of TCP as demonstrated by our XRD results.

The utilization of both ex vivo regional gene therapy and the 3D printed TCP scaffold resulted in 100% of rats healing the critical sized defect at 12 weeks in the experimental group and over half of the femoral defects actually had healed by 8 weeks. No defect healed in the three negative control groups. CT, histology, and histomorphometry confirmed the radiographic results and demonstrated significant new bone formation at the bone–scaffold interface and on the external surface of the scaffold. Biomechanical testing demonstrated similar stiffness between the experimental limb and the intact, contralateral limb indicating that the bone formed within and around the TCP scaffold deformed under initial torsional forces with similar properties to that of the intact contralateral femur. However, total energy to failure, peak torque, and peak displacement were significantly lower in the experimental limb. These lower values were not surprising since the animals were euthanized at 12 weeks after surgery and complete bone remodeling has not yet occurred in such a large bone defect. In addition, the 3D printed TCP scaffold had not resorbed and been replaced by bone at the 12-week time point, and this could alter the biomechanical properties of the healed defect. Near-complete resorption of the scaffold in vivo may take up to 86 weeks (Wiltfang et al., 2002). We were unable to perform biomechanical testing on the control groups because none of the defects completely healed.

There were no complications with the scaffold in the experimental group (group 1). Four of 15 (27%) negative control animals (groups 2–4) sustained proximal pin loosening. We hypothesize that motion at the proximal bone–scaffold interface generated a significant inflammatory reaction ranging from aseptic osteolysis (seen in two animals) to infection secondary to superficial migration of the loose proximal pins through the epidermal layer (seen in two animals). This only occurred proximally because the rat hip abductor mechanism attaches just proximal to the defect, resulting in significant motion at this site with ambulation. Our hypothesis is that the brittle nature of the TCP scaffold prevented a tight press-fit into the femoral defect and the motion lead to the generation of particulate debris and osteolysis. In the two animals with aseptic osteolysis, on radiographs and micro-CT imaging there was evidence of scaffold breakdown and proximal pin loosening (Figure 5); histologic evaluation demonstrated mild inflammation and TRAP straining was positive, confirming the presence of osteoclasts at the loose pin site. The presence of aseptic loosening due to osteolysis has not been previously observed in similar studies from our lab using non-3D printed TCP scaffolds. In the two animals that developed an infection, there was marked inflammation seen on histology, TRAP staining was negative, and the proximal pin sites were noted to be surrounded by purulent material during specimen harvest (data not shown). These findings have been seen before in similar studies from our lab using non-3D printed TCP scaffolds. Similar complications did not occur in the experimental group because bone formation at the proximal scaffold-defect interface stabilized the scaffold

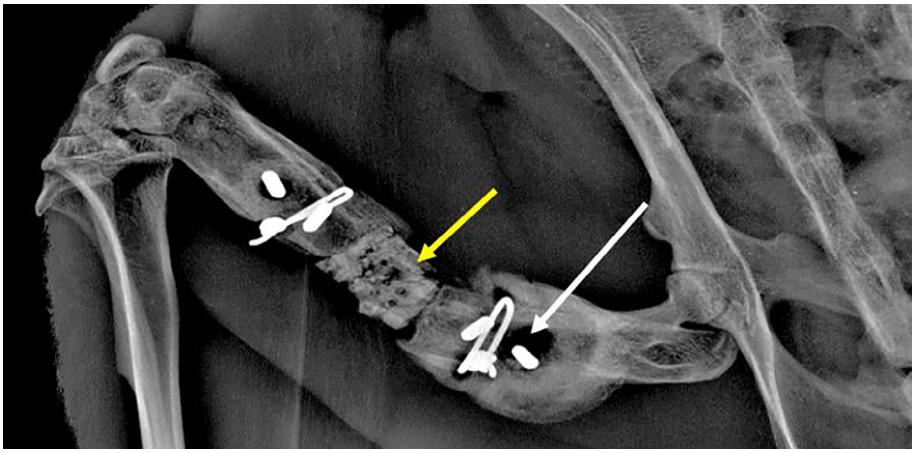

FIGURE 5 Plain radiograph demonstrating scaffold breakdown (yellow arrow) and proximal pin loosening with osteolysis at the proximal aspect of the bone defect (white arrow)

and prevented erosion of the scaffold from motion and subsequent pin loosening.

Although the results of this study are encouraging for developing a bone tissue engineering strategy through the utilization of both of ex vivo regional gene therapy and 3D printing, there are limitations. First, we chose TCP because it resembles the structure of cancellous bone, but it is a brittle material and may not have the biomechanical strength to resist large torsional forces seen in humans that may occur before bone remodeling is complete. Second, TCP can induce an osteolytic response from particulate debris when there is significant motion at the scaffold-defect interface, as demonstrated by two rats in the negative control groups. This osteolytic response could be a clinical problem in humans because this strategy would be used in cases where there was already structural bone loss. We are now assessing other scaffolds with different material properties in our laboratory. Third, we used RBMCs; further studies need to assess the compatibility of the TCP scaffold with human cells which would be used clinically.

5 | CONCLUSIONS

A multidisciplinary strategy utilizing a prolonged osteoinductive signal provided by transduced cells combined with a highly osteoconductive 3D printed scaffold represents a promising approach for bone tissue engineering in patients. This study demonstrates proof of concept for bone healing through the use of the combined strategy. The advent of 3D printing allows for scaffold design on a case by case basis to fit unique skeletal defects which is highly clinically relevant. In the clinical scenario a CT scan would be obtained to assess a large bone defect. This CT scan would be used as a template to create a 3D printed scaffold that fit into the bone defect and then could be loaded with the transduced cells. Further studies are needed to assess the compatibility of the 3D printed scaffold with transduced human cells, to optimize the 3D printed scaffold in terms of its biomechanical properties, and to investigate whether the 3D printed TCP scaffold provides added benefit in terms of bone formation and bone healing compared to a traditional collagen sponge or other carrier.

ACKNOWLEDGMENTS

None.

CONFLICT OF INTEREST

The authors have no conflicts of interest to disclose related to this work.

REFERENCES

Ahlmann, E., Patzakis, M., Roidis, N., Shepherd, L., & Holtom, P. (2002). Comparison of anterior and posterior iliac crest bone grafts in terms of harvest-site morbidity and functional outcomes. *The Journal of Bone and Joint Surgery. American Volume*, *84-A*(5), 716–720.

Alluri, R., Jakus, A., Bougioukli, S., Pannell, W., Sugiyama, O., Tang, A., … Lieberman, J. R. (2018). 3D printed hyperelastic "bone" scaffolds and regional gene therapy: A novel approach to bone healing. *Journal of Biomedical Materials Research. Part A*, *106*(4), 1104–1110.

Bougioukli, S., Evans, C. H., Alluri, R. K., Ghivizzani, S. C., & Lieberman, J. R. (2018). Gene therapy to enhance bone and cartilage repair in Orthopaedic surgery. *Current Gene Therapy*, *18*(3), 154–170.

Carragee, E. J., Hurwitz, E. L., & Weiner, B. K. (2011). A critical review of recombinant human bone morphogenetic protein-2 trials in spinal surgery: Emerging safety concerns and lessons learned. *The Spine Journal*, *11*(6), 471–491.

Carrodeguas, R. G., & De Aza, S. (2011). α-Tricalcium phosphate: Synthesis, properties and biomedical applications. *Acta Biomaterialia*, *7*(10), 3536–3546.

Castilho, M., Moseke, C., Ewald, A., Gbureck, U., Groll, J., Pires, I., … Vorndran, E. (2014). Direct 3D powder printing of biphasic calcium phosphate scaffolds for substitution of complex bone defects. *Biofabrication*, *6*(1), 15006.

Chan, D. S., Garland, J., Infante, A., Sanders, R. W., & Sagi, H. C. (2014). Wound complications associated with bone morphogenetic protein-2 in orthopaedic trauma surgery. *Journal of Orthopaedic Trauma*, *28*(10), 599–604.

Demiralp, B., Ege, T., Kose, O., Yurttas, Y., & Basbozkurt, M. (2014). Reconstruction of intercalary bone defects following bone tumor resection with segmental bone transport using an Ilizarov circular external fixator. *Journal of Orthopaedic Science*, *19*(6), 1004–1011.

Dorozhkin, S. V. (2012). Biphasic, triphasic and multiphasic calcium orthophosphates. *Acta Biomaterialia*, *8*(3), 963–977.

Esposito, M., Grusovin, M. G., Kwan, S., Worthington, H. V., & Coulthard, P. (2008). Interventions for replacing missing teeth: Bone

augmentation techniques for dental implant treatment. *Cochrane Database of Systematic Reviews*, *16*(3), CD003607.

Feeley, B. T., Conduah, A. H., Sugiyama, O., Krenek, L., Chen, I. S., & Lieberman, J. R. (2006). In vivo molecular imaging of adenoviral versus lentiviral gene therapy in two bone formation models. *Journal of Orthopaedic Research*, *24*(8), 1709–1721.

Garrison, K. R., Donell, S., Ryder, J., Shemilt, I., Mugford, M., Harvey, I., & Song, F. (2007). Clinical effectiveness and cost-effectiveness of bone morphogenetic proteins in the non-healing of fractures and spinal fusion: A systematic review. *Health Technology Assessment*, *11*(30), 1–150.

Hsu, W. K., Sugiyama, O., Park, S. H., Conduah, A., Feeley, B. T., Liu, N. Q., … Lieberman, J. R. (2007). Lentiviral-mediated BMP-2 gene transfer enhances healing of segmental femoral defects in rats. *Bone*, *40*(4), 931–938.

Ishihara, A., Zekas, L. J., Litsky, A. S., Weisbrode, S. E., & Bertone, A. L. (2010). Dermal fibroblast-mediated BMP2 therapy to accelerate bone healing in an equine osteotomy model. *Journal of Orthopaedic Research*, *28*(3), 403–411.

Jeon, O., Song, S. J., Kang, S. W., Putnam, A. J., & Kim, B. S. (2007). Enhancement of ectopic bone formation by bone morphogenetic protein-2 released from a heparin-conjugated poly(L-lactic-co-glycolic acid) scaffold. *Biomaterials*, *28*(17), 2763–2771.

Karageorgiou, V., & Kaplan, D. (2005). Porosity of 3D biomaterial scaffolds and osteogenesis. *Biomaterials*, *26*(27), 5474–5491.

Lee, J. W., Kang, K. S., Lee, S. H., Kim, J. Y., Lee, B. K., & Cho, D. W. (2011). Bone regeneration using a microstereolithography-produced customized poly(propylene fumarate)/diethyl fumarate photopolymer 3D scaffold incorporating BMP-2 loaded PLGA microspheres. *Biomaterials*, *32*(3), 744–752.

Lee, M. K., Deconde, A. S., Lee, M., Walthers, C. M., Sepahdari, A. R., Elashoff, D., … Aghaloo, T. (2015). Biomimetic scaffolds facilitate healing of critical-sized segmental mandibular defects. *American Journal of Otolaryngology*, *36*(1), 1–6.

Lieberman, J. R., Daluiski, A., & Einhorn, T. A. (2002). The role of growth factors in the repair of bone. Biology and clinical applications. *The Journal of Bone and Joint Surgery. American Volume*, *84-A*(6), 1032–1044.

Lieberman, J. R., Daluiski, A., Stevenson, S., Wu, L., McAllister, P., Lee, Y. P., … Witte, O. N. (1999). The effect of regional gene therapy with bone morphogenetic protein-2-producing bone-marrow cells on the repair of segmental femoral defects in rats. *The Journal of Bone and Joint Surgery. American Volume*, *81*(7), 905–917.

Mastrogiacomo, M., Muraglia, A., Komlev, V., Peyrin, F., Rustichelli, F., Crovace, A., & Cancedda, R. (2005). Tissue engineering of bone: Search for a better scaffold. *Orthodontics & Craniofacial Research*, *8*(4), 277–284.

Peterson, B., Zhang, J., Iglesias, R., Kabo, M., Hedrick, M., Benhaim, P., & Lieberman, J. R. (2005). Healing of critically sized femoral defects, using genetically modified mesenchymal stem cells from human adipose tissue. *Tissue Engineering*, *11*(1–2), 120–129.

Prockop, D. J. (1997). Marrow stromal cells as stem cells for nonhematopoietic tissues. *Science*, *276*(5309), 71–74.

Roskies, M., Jordan, J. O., Fang, D., Abdallah, M. N., Hier, M. P., Mlynarek, A., … Tran, S. D. (2016). Improving PEEK bioactivity for craniofacial reconstruction using a 3D printed scaffold embedded with mesenchymal stem cells. *Journal of Biomaterials Applications*, *31*(1), 132–139.

Sanz-Herrera, J. A., Doblaré, M., & Garcia-Aznar, J. M. (2010). Scaffold microarchitecture determines internal bone directional growth structure: A numerical study. *Journal of Biomechanics*, *43*(13), 2480–2486.

Seeherman, H. J., Li, X. J., Bouxsein, M. L., & Wozney, J. M. (2010). RhBMP-2 induces transient bone resorption followed by bone formation in a nonhuman primate core-defect model. *The Journal of Bone and Joint Surgery. American Volume*, *92*(2), 411–426.

Shen, H. C., Peng, H., Usas, A., Gearhart, B., Fu, F. H., & Huard, J. (2004). Structural and functional healing of critical-size segmental bone defects by transduced muscle-derived cells expressing BMP4. *The Journal of Gene Medicine*, *6*(9), 984–991.

Shim, J. H., Kim, S. E., Park, J. Y., Kundu, J., Kim, S. W., Kang, S. S., & Cho, D. W. (2014). Three-dimensional printing of rhBMP-2-loaded scaffolds with long-term delivery for enhanced bone regeneration in a rabbit diaphyseal defect. *Tissue Engineering. Part A*, *20*(13–14), 1980–1992.

Song, X., Chen, Y., Lee, T. W., Wu, S., & Cheng, L. (2015). Ceramic fabrication using mask-image-projection-based stereolithography integrated with tape-casting. *Journal of Manufacturing Processes*, *20*(3), 456–464.

Sugiyama, O., Sung An, D., Kung, S. P. K., Feeley, B. T., Gamradt, S., Liu, N. Q., … Lieberman, J. R. (2005). Lentivirus-mediated gene transfer induces long-term transgene expression of BMP-2 in vitro and new bone formation in vivo. *Molecular Therapy*, *11*(3), 390–398.

Temple, J. P., Hutton, D. L., Hung, B. P., Huri, P. Y., Cook, C. A., Kondragunta, R., … Grayson, W. L. (2014). Engineering anatomically shaped vascularized bone grafts with hASCs and 3D-printed PCL scaffolds. *Journal of Biomedical Materials Research. Part A*, *102*(12), 4317–4325.

Verettas, D. A., Galanis, B., Kazakos, K., Hatziyiannakis, A., & Kotsios, E. (2002). Fractures of the proximal part of the femur in patients under 50 years of age. *Injury*, *33*(1), 41–45.

Virk, M. S., Sugiyama, O., Park, S. H., Gambhir, S. S., Adams, D. J., Drissi, H., & Lieberman, J. R. (2011). "Same day" ex-vivo regional gene therapy : A novel strategy to enhance bone repair. *Molecular Therapy*, *19*(5), 960–968.

Wagoner Johnson, A. J., & Herschler, B. A. (2011). A review of the mechanical behavior of CaP and CaP/polymer composites for applications in bone replacement and repair. *Acta Biomaterialia*, *7*(1), 16–30.

Wang, H., Wu, G., Zhang, J., Zhou, K., Yin, B., Su, X., … Wu, Z. (2016). Osteogenic effect of controlled released rhBMP-2 in 3D printed porous hydroxyapatite scaffold. *Colloids Surfaces B Biointerfaces.*, *141*, 491–498.

Wang, J. C., & Kanim, L. E. (2003). A, Yoo S, Campbell P a, Berk AJ, Lieberman JR. effect of regional gene therapy with bone morphogenetic protein-2-producing bone marrow cells on spinal fusion in rats. *The Journal of Bone and Joint Surgery. American Volume*, *85-A*(5), 905–911.

Warnke, P. H., Seitz, H., Warnke, F., Becker, S. T., Sivananthan, S., Sherry, E., … Douglas, T. (2010). Ceramic scaffolds produced by computer-assisted 3D printing and sintering: Characterization and biocompatibility investigations. *Journal of Biomedical Materials Research. Part B, Applied Biomaterials*, *93*(1), 212–217.

Wiltfang, J., Merten, H. A., Schlegel, K. A., Schultze-Mosgau, S., Kloss, F. R., Rupprecht, S., & Kessler, P. (2002). Degradation characteristics of alpha and beta tri-calcium-phosphate (TCP) in minipigs. *Journal of Biomedical Materials Research*, *63*(2), 115–121.

Woodfield, T. B., Malda, J., de Wijn, J., Péters, F., Riesle, J., & van Blitterswijk, C. A. (2004). Design of porous scaffolds for cartilage tissue engineering using a three-dimensional fiber-deposition technique. *Biomaterials*, *25*(18), 4149–4161.

Younger, E. M., & Chapman, M. W. (1989). Morbidity at bone graft donor sites. *Journal of Orthopaedic Trauma*, *3*(3), 192–195.

How to cite this article: Alluri R, Song X, Bougioukli S, et al. Regional gene therapy with 3D printed scaffolds to heal critical sized bone defects in a rat model. *J Biomed Mater Res*. 2019; 107A:2174–2182. https://doi.org/10.1002/jbm.a.36727